Electronic Supplementary Material (ESI) for Chemical Communications.
This journal is © The Royal Society of Chemistry 2015

Electronic Supplementary Information

A novel p-$LaFeO_3$/n-Ag_3PO_4 heterojunction photocatalyst for phenol degradation under visible light irradiation

Jun Yang,[a] Ruisheng Hu,*[a] Wanwan Meng,[a] and Yanfei Du[a]

[a]Key Laboratory of Chemistry and Physics of Rare Earth Materials, School of Chemistry and Chemical Engineering, Inner Mongolia University, Inner Mongolia, 010021, China.

*To whom the correspondence should be addressed. E-mail: cehrs@imu.edu.cn. (Ruisheng Hu)

● Experimental Section

1.1 Preparation of photocatalysts

All chemical regents of analytical grade were used without any purification.

Synthesis of pure phase $LaFeO_3$

$LaFeO_3$ was prepared by the citric acid sol-gel method. Stoichimetric amounts of $La(NO_3)_3 \cdot 6H_2O$ and $Fe(NO_3)_3 \cdot 9H_2O$ (molar ratio=1:1) were dissolved in deionized water and mixed with appropriate citric acid as the complexing agent. The mixed solution was placed in a thermostatic water bath at 70℃ with magnetic stirring until it formed a viscous wet gel. Then the wet gel was dried at 100℃ in a drying oven to get the xerogel. Finally, the xerogel was calcined first at 500℃ for 3 h, then at 700℃ for 3 h.

Preparation of p-$LaFeO_3$/n-Ag_3PO_4 composite photocatalysts

$LaFeO_3/Ag_3PO_4$ composite with different mass ratio were synthesized by an in-situ precipitation method in the silver-ammine solution. At First, a certain amount of $AgNO_3$ was fully dissolved in 100 ml of distilled water, and stirred for 10 min. Then, 10% mass fraction of ammonia solution was added into above solution under stirring condition to obtain the silver-ammonia complex. Meanwhile，a certain amount of as-prepared $LaFeO_3$ was dispersed in 100 ml distilled water and stirred for 20 min, then sonicated for 10 min. Subsequently, the suspension of $LaFeO_3$ was slowly added to the silver-ammine solution and stirred for 6 h, then sonicated for 30 min, Finally, under continuous stirring 1mol/L Na_2HPO_4 was added into the above mixture drop by drop and kept stirring for 10 h. The obtained precipitates were washed with distilled water and anhydrous ethyl alcohol for three times and then dried at 50℃ overnight to get $LaFeO_3/Ag_3PO_4$ composite photocatalysts. Depending on the mass fraction of Ag_3PO_4 in the composite system, different nanocomposites can be synthesized, respectively. The series of photocatalysts prepared were labeled as LFO/APO-X（LFO and APO are the abbreviations for $LaFeO_3$ and Ag_3PO_4, X represents the mass fraction of Ag_3PO_4 in the composite system. X= 20%, 40%, 60%, 80%).

For comparison, pure phase Ag_3PO_4 was also prepared under the same condition without adding $LaFeO_3$.

1.2 Characterizations of photocatalysts

The X-ray powder diffraction (XRD) data of the as-prepared samples were recorded by a PANalytical Empyrean diffractometer (Netherlands) with a copper target. Particle sizes and morphologies of the samples were determined using scanning electron microscopy (SEM) on a HITACHI S-4800 apparatus with an acceleration voltage of 20.0 kV and high-Resolution transmission Electron Microscope (HRTEM) analysis was performed on a JEM-2010 apparatus with an acceleration voltage of 200 kV. The optical diffuse reflectance spectra were measured using a Lambda 750s UV/vis spectrometer using $BaSO_4$ for the corrected baseline at room temperature. X-ray photoelectron spectroscopy (XPS) was performed on a Thermo ESCALAB 250 spectrometer with Al Kα (1486.6eV). To compensate surface charges effects, all the binding energies were referenced to the C1s peak at 284.6eV. A NOVA 4200e (Quantachrome) instrument was used to measure the Brunauer-Emmett-Teller (BET) surface areas of the samples at liquid nitrogen temperature (77 K). Specific surface area calculations were made using Brunauer-Emmett-Teller (BET) method at the relative pressure (P/P0) between 0.05 and 0.35. The photoluminescence (PL) spectra were performed by using a Hitachi F-4600 spectrophotometer with an excitation wavelength of 350 nm.

Photoelectrochemical measurements The photocurrent experiments were performed using an Auto-lab model AUT302N.FRA32M.V electrochemical workstation with a three-electrode cell. 10 mg of the prepared sample was added into 2 mL of isopropanol to form a uniform suspension after 30 min of ultrasonic treatment. The suspension was coated on a piece of FTO glass (1×1.5 cm^2) with 0.2 cm^2 restricted by a sticky tape, then dried at room temperature for 24 h. The FTO glass, platinum wire and Ag/AgCl electrodes were used as working, counter and reference electrodes, respectively. 500 W Xe lamp was used as the lightsource. The electrolyte solution was a NaOH aqueous solution (0.2mol L^{-1}).

The surface photovoltage (SPV) measurement system included a source of monochromatic light, a lock-in amplifier (SR830-DSP) with a light chopper (SR540), a photovoltaic cell, and a computer. A 500 W xenon lamp and a double-prism monochromator (Zolix SBP500) provide monochromatic light as the source light. The samples were studied without further treatment during the SPV measurement, and the contact between samples and the indium tin oxide (ITO) electrode was not ohmic when we carried out the measurement of surface photovoltage. The construction of the photovoltaic cell is a sandwichlike structure of ITO-sample-ITO. We put the powder sample on the ITO electrode and press it with another ITO electrode to obtain a film composed of the powder sample.

1.3 Photocatalytic activity test

The photocatalytic activity was evaluated by the degradation of aqueous phenol solution (20 mg/L) at room temperature under visible light irradiation (CEL-LAX500, Beijing AuLight Ltd. Co.). The reaction was carried out under the condition of air ventilation and the magnetic stirring. In detail, the procedure of the degradation experiment was as follows: 50 mg of the prepared photocatalyst was dispersed in a quartz tube containing 50 ml phenol aqueous solution (20 mg/l). Then the suspension was kept stirring in the dark for 30 min to reach the adsorption-desorption equilibrium on the catalyst surface. The suspension was irradiated by a 500 W xenon lamp with a filter ($\lambda \geq 420$ nm). After that, 5 mL of the suspensions was extracted at given intervals and subsequently centrifuged. The phenol concentration was determined by using an ultraviolet spectrophotometer (UV-7504PC) at a wavelength of 270 nm based on the Lambert- Beer law. The degradation efficiency of phenol was calculated according to the equation: $\eta = (C_0 - C_t)/C_0 \times 100\%$, where η is the photocatalytic efficiency, C_0 is the absorbance intensity of the phenol solution after the adsorption-desorption equilibrium, and C_t is the absorbance intensity of phenol after irradiation.

In addition, a series of experiments were conducted to investigate the primary radical species during the degradation of phenol over the $LaFeO_3/Ag_3PO_4$ samples via introducing various scavengers into the phenol solution. The experimental procedure was similar to the above photodegradation experiment. Briefly, the phenol photodegradation was repeated by adding 1mmol of benzoquinone (BQ) as a superoxide radical scavenger ($O_2^{\bullet}$), 10 mmol of tert-butyl alcohol (TBA) as a hydroxyl radical scavenger ($^{\bullet}OH$) and 10 mmol of ammonium oxalate (AO) as a hole (h^+) scavenger.[1]

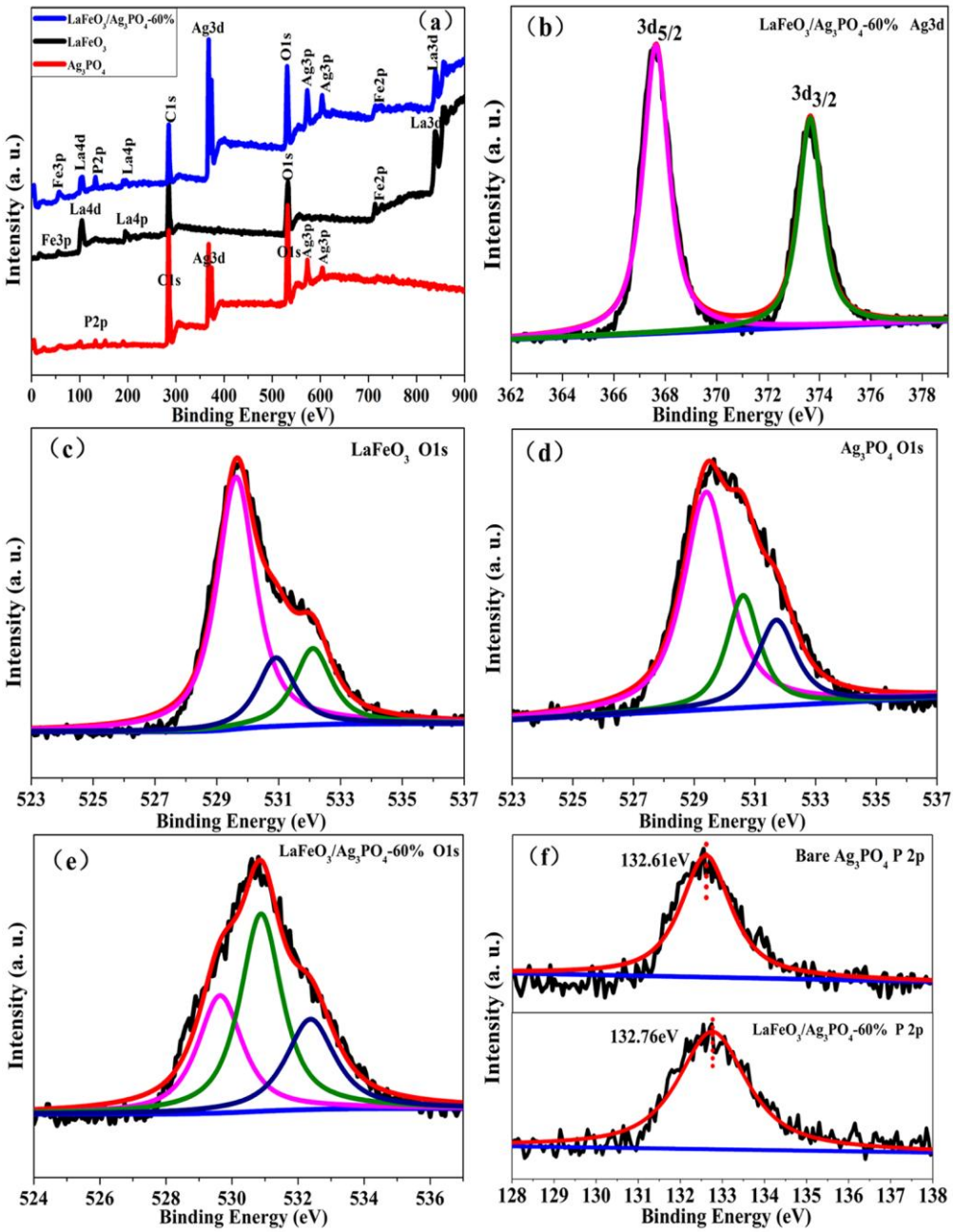

Fig.S1 XPS spectra: (a) The whole scanning XPS spectra of bare $LaFeO_3$, Ag_3PO_4 and $LaFeO_3/Ag_3PO_4$-60%, respectively; (b) the high-resolution regional spectra of Ag 3d orbital of the $LaFeO_3/Ag_3PO_4$-60% composite catalyst; (c), (d) and (e) The XPS spectra of O1s orbital of $LaFeO_3$, Ag_3PO_4 and $LaFeO_3/Ag_3PO_4$-60%, respectively; (f) P 2p XPS spectra of the bare Ag_3PO_4 and $LaFeO_3/Ag_3PO_4$-60%, respectively.

It is well known that the surface chemical composition and element chemical state of the photocatalyst have a great influence on the photocatalytic reaction, so the

XPS technique was carried out. Fig. S1 (a) shows the XPS survey spectra of pure phase $LaFeO_3$, bare Ag_3PO_4 and $LaFeO_3/Ag_3PO_4$-60% composite catalyst, respectively. It can be seen that all the peaks can be assigned to Ag, P, O and C elements for bare Ag_3PO_4, La, Fe, O and C elements for bare $LaFeO_3$, and Ag, P, La, Fe, O and C elements for $Ag_3PO_4/LaFeO_3$-60% composite.

Fig.S1 (b) displays the high-resolution Ag 3d XPS spectra of the fresh $Ag_3PO_4/LaFeO_3$-60% composite catalyst. It can be seen that two binding energy peaks appear at 367.6eV and 373.6eV corresponding to Ag $3d_{5/2}$ and Ag $3d_{3/2}$, respectively, which are attributed to Ag^+.[2] There are no XPS spectra of Ag nanocrystals existing on the surface of Ag_3PO_4, indicating that no Ag^0 was formed during the preparation and components of the composite at the surface are Ag_3PO_4 and $LaFeO_3$.

Surface oxygen species play an important role in the photocatalytic process, so the O1s XPS spectra are analyzed, as depicted in Fig.S1 (c), (d) and (e) corresponding to $LaFeO_3$、Ag_3PO_4 and $LaFeO_3/Ag_3PO_4$-60%, respectively. It can be seen that all the O1s XPS peaks can be well-reproduced by three Lorentzian-Gaussian lines, which implies that there are three kinds of surface oxygen species in the samples. The binding energy at about 529.65eV belongs to the lattice oxygen atoms (O_{lat}). The main peak at 531.28eV can be assigned to hydroxyl oxygen (O_{OH}). The binding energy of 532.47eV is ascribed to surface adsorbed oxygen (O_{O2}).[3] The peak fitting analysis data of the three oxygen species are shown in table S1. It can be seen that both the hydroxyl oxygen and the absorbed oxygen content of the heterojunction composite are higher than the individual $LaFeO_3$ and Ag_3PO_4. According to the reported literature,[4,5] the hydroxyl oxygen and the adsorbed oxygen can produce a mass of hydroxyl radicals and hydrogen peroxide, which have strong oxidization property and then are very beneficial to the photocatalytic reaction.

In addition, the high-resolution P 2p spectra of the bare Ag_3PO_4 and fresh $Ag_3PO_4/LaFeO_3$-60% composite are shown in Fig.S1 (f). The peak of bare Ag_3PO_4 at 132.61 eV, which is lower than the peak 132.76 eV of $Ag_3PO_4/LaFeO_3$-60% composite. The binding energy shift of P 2p reveals a strong interaction between

$LaFeO_3$ and Ag_3PO_4 in the heterojunction structure, which implies the existence of electron transfer and chemical bonds between the two components.[6,7]

Table S1. Oxygen species content of $LaFeO_3$, Ag_3PO_4 and $LaFeO_3/Ag_3PO_4$-60%

Catalysts	O_{lat} (eV)/O_{tal}	O_{OH} (eV)/O_{tal}	O_{O2} (eV)/O_{tal}
$LaFeO_3$	64.56%	16.73%	18.71%
Ag_3PO_4	58.47%	21.78%	19.75%
$LaFeO_3/Ag_3PO_4$-60%	30.86%	40.40%	28.74%

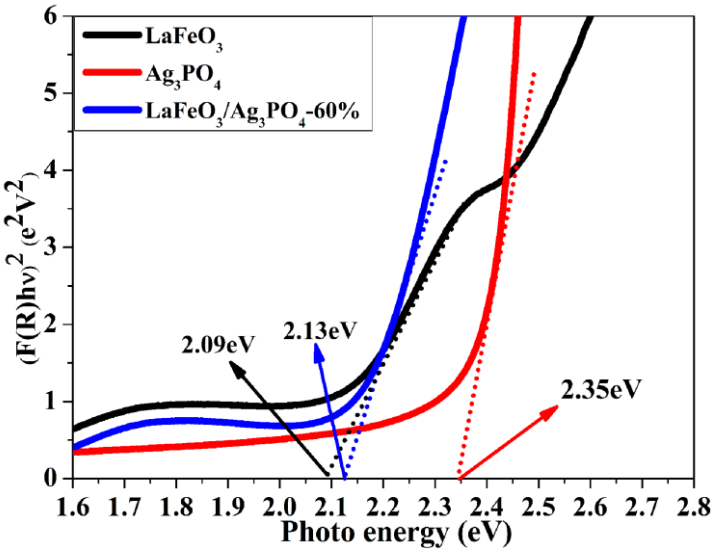

Fig.S2 Optical band gap energies of bare $LaFeO_3$, Ag_3PO_4 and $LaFeO_3/Ag_3PO_4$-60% composite.

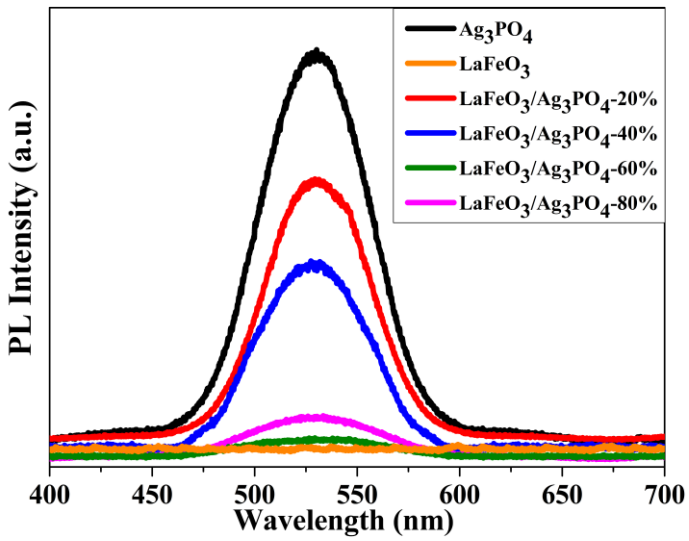

Fig.S3 Photoluminescence spectra of pure Ag_3PO_4, pure $LaFeO_3$, $LaFeO_3/Ag_3PO_4$-20%, $LaFeO_3/Ag_3PO_4$-40%, $LaFeO_3/Ag_3PO_4$-60%, and $LaFeO_3/Ag_3PO_4$-80%

It is known that the recombination of electron-hole pairs can release energy in the form of fluorescence emission. Lower PL intensity indicates lower recombination of charge carriers. Therefore, PL analysis can be regarded as a direct approach to study the separation efficiency of photo-generated carriers.[8,9] As clearly seen in Fig. S3, for the single $LaFeO_3$, there is no obvious fluorescence signal. However, for pure Ag_3PO_4 and $LaFeO_3/Ag_3PO_4$ composites, a strong emission peak at about 530 nm is observed, which is caused by the recombination of photo-excited electrons and holes.[10,11] The PL intensity of pure Ag_3PO_4 is higher than that of $LaFeO_3/Ag_3PO_4$ hybrids, implying that the heterojunction could promote the separation of charge carriers.

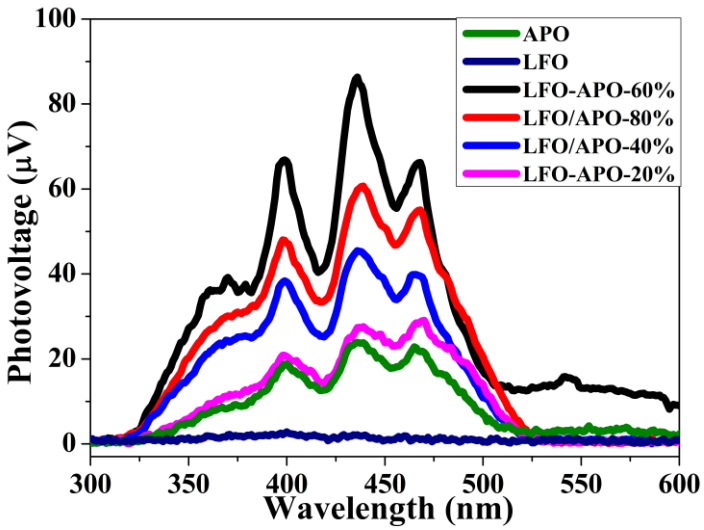

Fig. S4 The surface photovoltage (SPV) spectra of Ag_3PO_4, $LaFeO_3$, and $LaFeO_3/Ag_3PO_4$ composites

To further investigate the separation and transfer process of photo-induced charges, SPV measurement was carried out, which can provide a direct evidence of the band-gap transition.[12] Fig. S4 presents the SPV spectra of Ag_3PO_4, $LaFeO_3$ and $LaFeO_3/Ag_3PO_4$ composites. The SPV response of single Ag_3PO_4 takes place in the range of 300-530 nm, which is attributed to electrons transition from valence band to conduction band. Obviously, the SPV responses of $LaFeO_3/Ag_3PO_4$ composites are all stronger than that of pure Ag_3PO_4 and the p-n heterojunction composites extend the response range of visible light in different degrees, which is consistent with the test results of UV-vis diffuse reflectance spectra. However, the SPV response of $LaFeO_3$ is almost undetectable, which provides an evidence of the low separation efficiency of charge carriers in $LaFeO_3$. $LaFeO_3/Ag_3PO_4$ composites exhibit a similar SPV response to Ag_3PO_4, suggesting the photovoltage response of composites mainly arises from Ag_3PO_4.[13] Unlike the UV–vis spectra, which involves all kinds of photon absorption, the SPV is only sensitive to the electron transition-related process and charge carriers' separation. On this basis, it is supposed that a stronger SPV response intensity indicates a higher separation efficiency of photo-induced charges.[14,15] The SPV measurements are all under the same condition, so the obvious SPV response difference between Ag_3PO_4 and $LaFeO_3/Ag_3PO_4$ could be attributed to the interfacial interaction between Ag_3PO_4 and $LaFeO_3$. We speculate that a built-in electric field is

formed at the interface of Ag_3PO_4 and $LaFeO_3$ in the process of preparation, which makes the electron-hole pairs can be separated effectively. In addition, it is interesting that the response intensity of $LaFeO_3/Ag_3PO_4$-60% composite is higher than that of $LaFeO_3/Ag_3PO_4$-20% and $LaFeO_3/Ag_3PO_4$-40%, but lower than $LaFeO_3/Ag_3PO_4$-80% composite. It is just maybe induced by the agglomeration of $LaFeO_3$ particles, leading to a decrease of photons to reach the interface and an increase of migration distance of photo-induced charges. This is consistent with the results of photo-catalytic activity test.

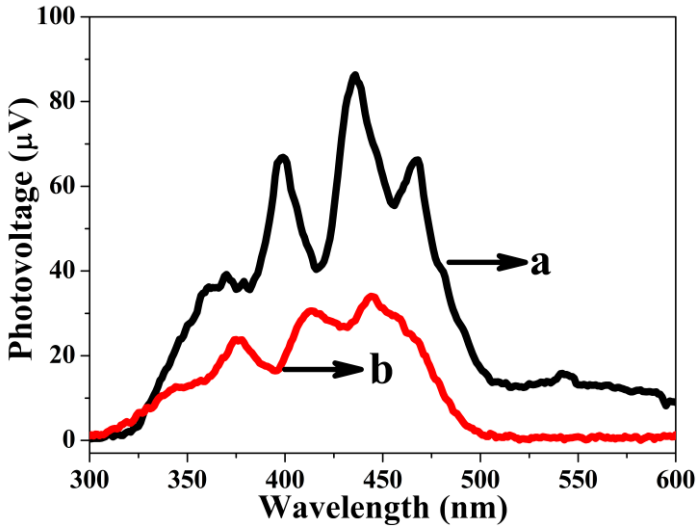

Fig. S5 SPV spectra of (a) $LaFeO_3/Ag_3PO_4$-60% composite and (b) mechanical mixture $LaFeO_3$ and Ag_3PO_4 (the mass ratio of Ag_3PO_4 is 60%).

Figure S5 shows the SPV spectra of $LaFeO_3/Ag_3PO_4$-60% composite and mechanical mixed Ag_3PO_4 and $LaFeO_3$ (the mass ratio of Ag_3PO_4 is 60%). The SPV response intensity of the mechanical mixture is much lower than that of $LaFeO_3/Ag_3PO_4$-60% composite. The result further confirmed the existence of the interfacial built-in electric field, which can promote the separation of photo-generated charge carriers.

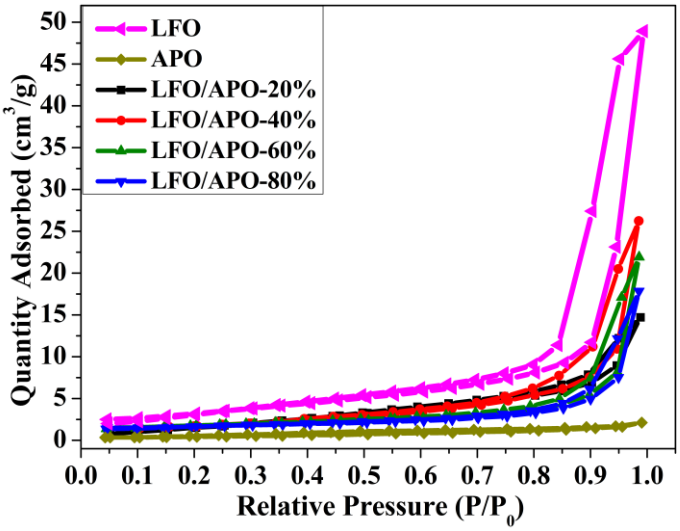

Fig. S6 Nitrogen adsorption-desorption isotherms of Ag_3PO_4, $LaFeO_3$ and $LaFeO_3/Ag_3PO_4$ composites.

Fig. S6 presents the N_2 adsorption-desorption isotherms of pure Ag_3PO_4, pure $LaFeO_3$ and $LaFeO_3/Ag_3PO_4$ composites. The single Ag_3PO_4 exhibits a very small hysteresis loops. As a contrast, $LaFeO_3$ and $LaFeO_3/Ag_3PO_4$ composites display typical type IV isotherms with a H3 hysteresis loop according to the IUPAC classification,[16] indicating that the samples have mesoporous structures. The BET surface area values are 1.54 m^2/g, 11.86 m^2/g ,7.51 m^2/g ,6.20 m^2/g ,5.81 m^2/g ,5.25 m^2/g and 5.28 m^2/g for Ag_3PO_4, $LaFeO_3$, $LaFeO_3/Ag_3PO_4$-20%, $LaFeO_3/Ag_3PO_4$-40%, $LaFeO_3/Ag_3PO_4$-60%, and $LaFeO_3/Ag_3PO_4$-80%, respectively. Obviously, there are only small differences among the surface area values of $LaFeO_3/Ag_3PO_4$ composites. It can be speculated that the different photocatalytic activity of the samples could not be determined by the BET surface areas in the process of phenol removal.

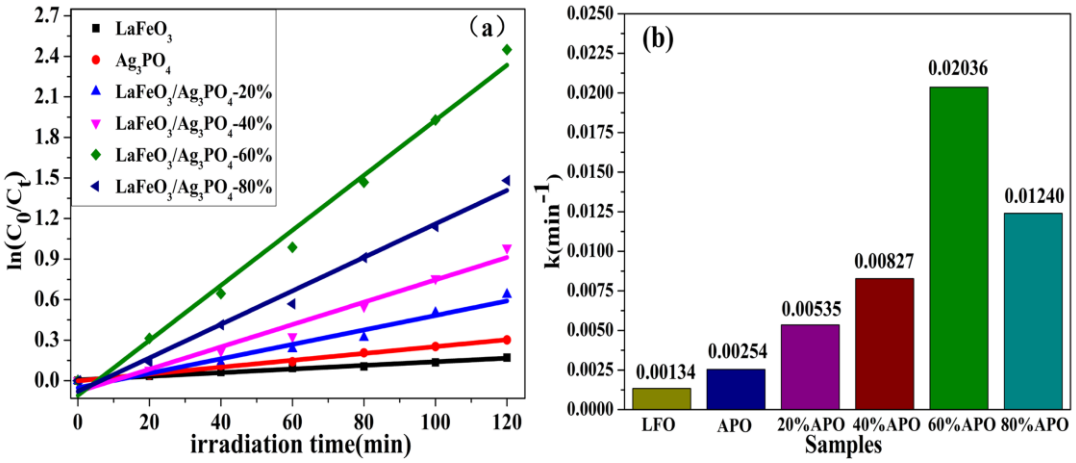

Fig. S7 (a) the corresponding kinetics of phenol degradation; (b) Plots of rate constant of phenol degradation over the photocatalysts

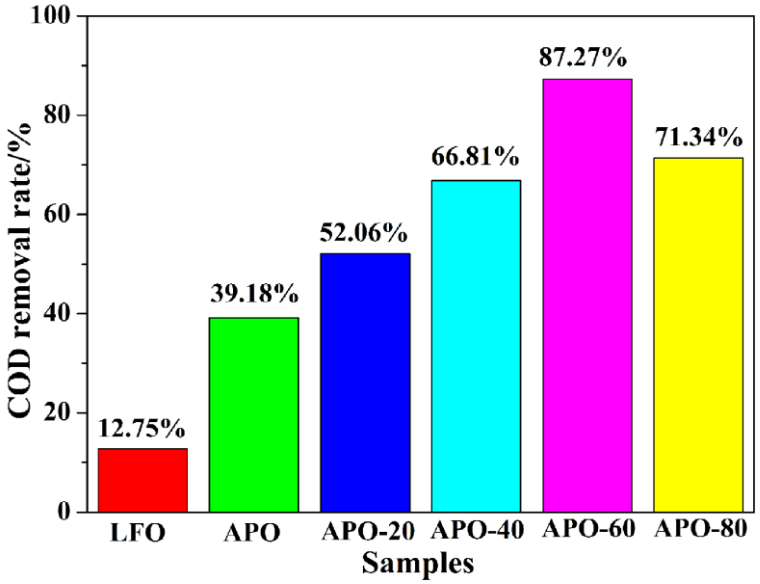

Fig.S8 COD removal rate of the phenol solution

Chemical oxygen demand (COD) is the oxygen equivalent to form CO_2 and H_2O during the mineralization process of organic substance. It is one of the important water pollution parameters, which has been widely used in the evaluation of organic

compounds in waste water. The COD was determined by using potassium dichromate oxidation method. The COD removal rate was calculated according to the formula: $\Psi(\%)=(C_0-C_t)/C_0\times100\%$, where ψ is the COD removal rate, C_0 (mg/L) is the concentration of COD before the photocatalytic reaction, and C_t (mg/L) is the concentration of COD after the photocatalytic reaction.[17,18] Obviously, the higher COD removal rate indicates the higher organic substance mineralization rate during the photocatalytic degradation progress. Fig.S8 shows the results of the COD removal rate after two hour visible light irradiation, it can be seen that the composite $LaFeO_3/Ag_3PO_4$-60% shows the highest COD removal rate, which is much higher than the single $LaFeO_3$ and Ag_3PO_4.

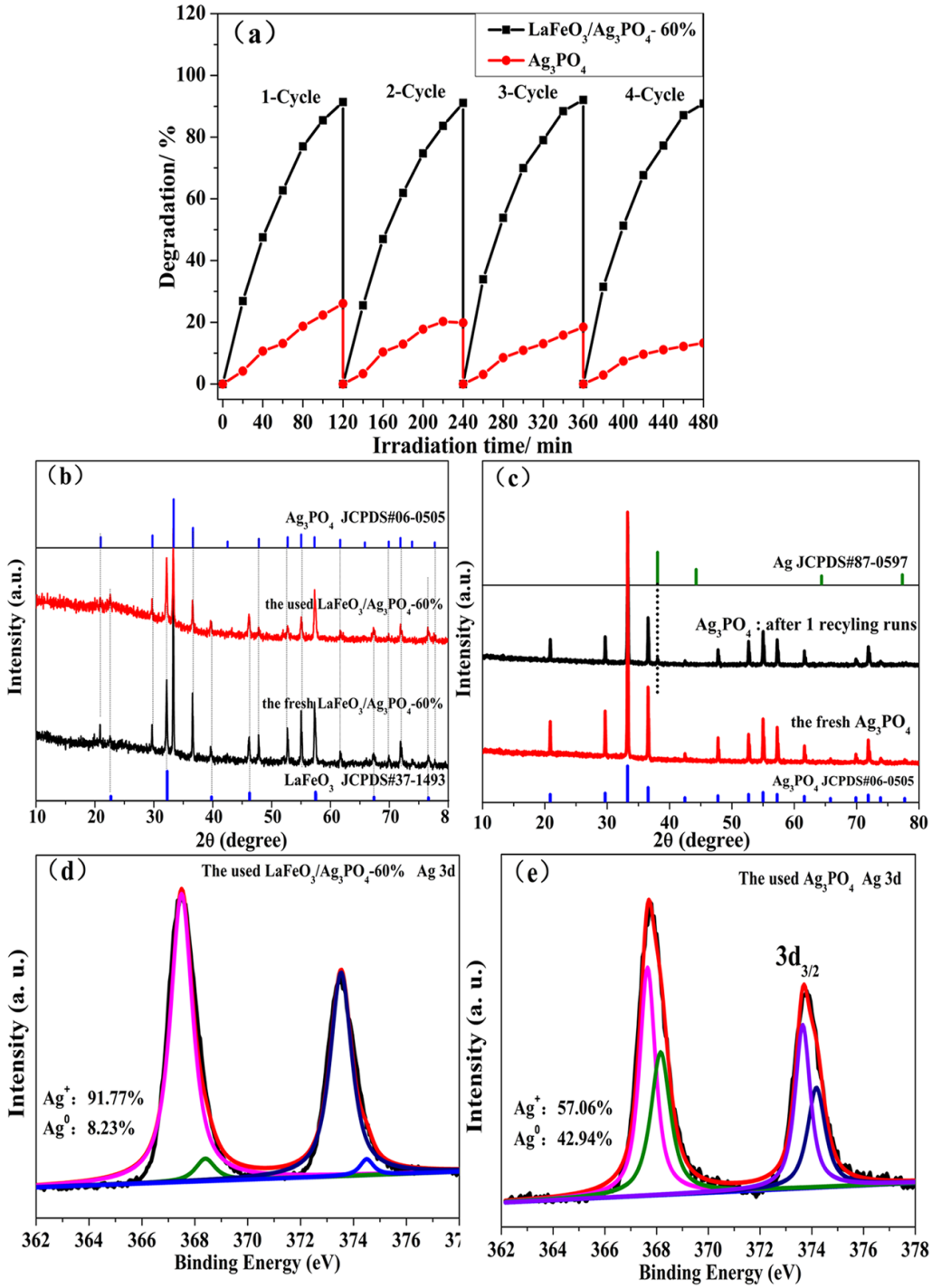

Fig. S9 (a) Recycling tests of Ag_3PO_4 and $LaFeO_3/Ag_3PO_4$-60% for the degradation of phenol under visible light irradiation. (b) XRD patterns of the fresh and the used $LaFeO_3/Ag_3PO_4$-60% after 4 recycling runs. (c) XRD patterns of the fresh and the used Ag_3PO_4 after 1 recycling run. (d) Ag 3d XPS spectra of the used $LaFeO_3/Ag_3PO_4$-60% after 4 recycling runs; (e) Ag 3d XPS spectra of Ag_3PO_4 after 1 recycling run.

The stability of Ag_3PO_4 is an important issue in the photodegradation reaction, so the stability of the $LaFeO_3/Ag_3PO_4$-60% composite and fresh Ag_3PO_4 catalyst was investigated. As shown in Fig.S9 (a), it can be seen that the composite catalyst $LaFeO_3/Ag_3PO_4$-60% exhibited excellent photocatalytic stability for the degradation of phenol under visible light. At the fourth run, the degradation rate of phenol is still up to 90.85% under visible light irradiation for 120 min, which is similar with the first run (91.37%). However, the degradation rate of bare Ag_3PO_4 is obviously decreased after four recycling runs, which is down to 29.72% from the first time of 55.15%.

In addition, the XRD and XPS spectra of bare Ag_3PO_4 and $LaFeO_3/Ag_3PO_4$-60% composite before and after the photocatalytic reaction are analyzed, which are shown in Fig.S9 (b, c, d, e). Fig.S9 (b) shows the XRD patterns of the fresh and the used $LaFeO_3/Ag_3PO_4$-60% catalyst, it can be seen that $LaFeO_3/Ag_3PO_4$-60% composite still exhibits a coexistence of Ag_3PO_4 and $LaFeO_3$ phases and no impurity phase diffraction peaks are detected and the difference is focused on the intensity of the corresponding peaks. However, a diffraction peak at 38.1 °attributed to metallic Ag is found in the used Ag_3PO_4. The formation of metallic Ag would decrease the photocatalytic performance of Ag_3PO_4,[19] so the high-resolution regional spectra of Ag 3d orbital of the $LaFeO_3/Ag_3PO_4$-60% composite catalyst was further investigated. Fig. S9 (d) and (e) shows the Ag3d XPS spectra of the used $LaFeO_3/Ag_3PO_4$-60% and Ag_3PO_4 catalysts, respectively. The Ag 3d spectra include two kinds of peaks: One kind is at about 368.42 eV and 374.49 eV, which can be attributed to the Ag $3d_{5/2}$ and Ag $3d_{3/2}$ of Ag^0, respectively; the other kind contains two weak peaks at 367.48 eV and 373.51 eV which should be ascribed to the Ag $3d_{5/2}$ and Ag $3d_{3/2}$ of Ag^+, respectively.[2] The calculated mole content of Ag^0 was 42.94% of the total silver element on the surface of Ag_3PO_4 catalyst, while only 8.23% of Ag^0 was found on the surface of $LaFeO_3/Ag_3PO_4$-60% catalyst after four runs. That is to say, much less metallic Ag was formed on the surface of $LaFeO_3/Ag_3PO_4$ composite during the degradation process than that on the surface of Ag_3PO_4 catalyst. Thus it can be seen that the construction of heterogeneous $LaFeO_3/Ag_3PO_4$ can improve the stability of single Ag_3PO_4, which is beneficial for the photocatalytic degradation process.

The potentials of the conduction band (CB) and valence band (VB) edges of $LaFeO_3$ and Ag_3PO_4 can be obtained according to the Mulliken electronegativity theory, which is shown as follow in Eq. S(1) and Eq. S(2):

$E_{VB}= \chi - E_C+0.5Eg$ Eq. S(1)

$E_{CB}=E_{VB}-E_g,$ Eq. S(2)

where E_{VB} and E_{CB} stand for the conduction band and valence band edge potential respectively, χ is the absolute electronegativity of the semiconductor, which is the geometric mean of the electronegativities of the constituent atoms,[20] and E_c is the energy of free electrons on the hydrogen scale (about 4.5eV vs NHE),[21] Eg is the band gap of semiconductor. The X value is calculated to be 5.96 eV for Ag_3PO_4 and 5.70 eV for $LaFeO_3$, respectively.

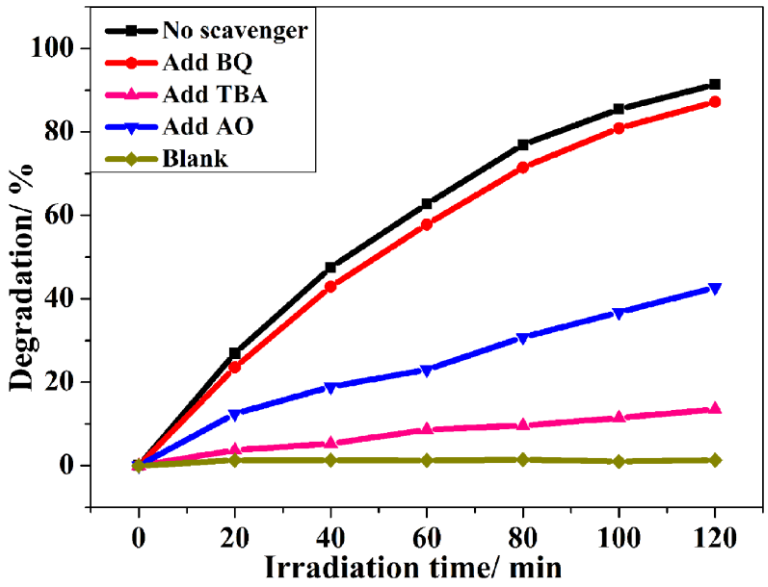

Fig. S10 Effects of different scavengers on phenol degradation in the presence of $LaFeO_3/Ag_3PO_4$-60% under visible light irradiation.

The free radicals capture experiments were conducted by adding active species scavengers using phenol photo-degradation as the model reaction. Briefly, the phenol photodegradation was repeated by adding 1mmol of benzoquinone (BQ) as a

superoxide radical scavenger ($O_2^{\bullet}$), 10 mmol of tert-butyl alcohol (TBA) as a hydroxyl radical scavenger (•OH) and 10 mmol of ammonium oxalate (AO) as a hole (h+) scavenger.[1] As shown in Fig. S6, the photodegradation of phenol was apparently inhibited when AO and TBA were added, while there was no obvious photodegradation reduction with the addition of BQ. This phenomenon gives evidence that the degradation of phenol is dominated by the oxidation reaction of hydroxyl radicals and direct hole oxidation.

References

1 Y. G. Su, L. M. Peng, J. W. Guo, S. S. Huang, L. Lv and X. J.Wang, *J. Phys. Chem. C,* 2014, **118**, 10728.

2 R. F. Dong, B. Z. Tian, C. Y. Zeng, T. Y. Li, T. T. Wang and J. L. Zhang, *J. Phys. Chem. C,* 2013, **117**, 213.

3 Z. Z. Zhang, J. L. Long, X. Q. Xie, H. Q. Zhuang, Y. G. Zhou, H. Lin, R. S. Yuan, W. X. Dai, Z. X. Ding, X. X. Wang and X. Z. Fu, *Appl. Catal., A*, 2012, **425-426**, 117.

4 M. S. Lazarus and T. K. Sham, *Chem. Phys. Lett.,* 1982, **92**, 670.

5 T. T.Wang, J. Y. Lang, Y. J. Zhao, Y. G. Su, Y. X. Zhao and X.J. Wang, *CrystEngComm,* 2015, **17**, 6651.

6 F. T. Li, Y. Zhao, Q. Wang, X. J. Wang, Y. J. Hao, R. H. Liu and D. S. Zhao, *J. Hazard. Mater.,* 2015, **283**, 371.

7 T. Yan, M. Sun, H. Y. Liu, T. T. Wu, X. J. Liu, Q. Yan, W. G. Xu and B. Du, *J. Alloys Compd.,* 2015, **634**, 223.

8 S. Usai, S. Obregón, A. I. Becerro, and G. Colón, *J. Phys. Chem. C* 2013, **117**, 24479.

9 J. G. Yu, H. G. Yu, B. Cheng, X. J. Zhao, J. C. Yu, and W. K. Ho, *J. Phys. Chem. B* 2003, **107**, 13871.

10 S. S. Patil, M. S. Tamboli, V. G. Deonikar, G. G. Umarji, J. D. Ambekar, M. V. Kulkarni, S. S. Kolekar, B. B. Kale and D. R. Patil, *Dalton Trans.*, 2015, **44**, 20426

11 Q. Liang, Y. Shi, W. Ma, Z. Li and X. Yang, *Phys. Chem.Chem. Phys.*, 2012, **14**, 15657.

12 X. Wei, T. F. Xie, L. L. Peng, W. Fu, J. S. Chen, Q. Gao, G. Y. Hong, D. J. Wang, *J. Phys. Chem. C.*, 2011, **115**, 8637.

13 Y. Bessekhouad, D. Robert, and J. V. Weber, *Catal. Today* 2005, **101**, 315.

14 T. F. Xie, D. J. Wang, S. M. Chen, and T. J. Li, *Thin Solid Films* 1998, **327−329**, 415.

15 Z. Y. Liu, D. D. L. Sun, P. Guo, and J. O. Leckie, *Nano Lett.*, 2007, 7, 1081.

16 K. S. W. Sing, D. H. Everett, R. A. W. Haul, L. Moscou, R. A. Pierotti, J. Rouquerol and T. Siemieniewska, *Pure Appl. Chem.*, 1985, **57**, 603.

17 Z. F. Ye, Q. L. Zhao, M. H. Zhang and Y. C. Gao, *J. Hazard. Mater.*, 2011, **186**, 1351.

18 N. Mohaghegh, E. Rahimi and M. R. Gholami, *Mater. Sci. Semicond. Process.*, 2015, **39**, 506.

19 Y. P. Bi, S. X. Ouyang, J. Y. Cao and J.H. Ye, *Phys. Chem. Chem. Phys.*, 2011, **13**, 10071.

20 X. Xin, J. Y. Lang, T. T Wang, Y. G. Su, Y. X. Zhao and X. J. Wang, *Appl. Catal., B*, 2016, **181**, 197.

21 Y. G. Su, X. Xin, Y. F. Wang, T. T. Wang and X. J. Wang, *Chem. Commun.*, 2014, **50**, 4200.